Probing the Effects of Structural Variation on Concerted Proton-Electron Transfer

Melissa Vettleson

Candidate for the degree:

Bachelor of Sciences

Submitted for:

Departmental Distinction in Chemistry

Dr. Ian Rhile, PhD

Dr. Christopher Graves, PhD

Dr. Bryce Brylawski, PhD

F. Wilbur Gingrich Library
Special Collections Department
Albright College

Release of Senior Thesis

I hereby deliver, give, and transfer property, rights, interest in and legal rights thereto which I had, have, or may have concerning the Senior Honors Thesis described below to the Special Collections Department of the F. Wilbur Gingrich Library at Albright College as an unrestricted gift. While copyright privileges will remain with me, the author, all privileges to reproduce, disseminate, or otherwise preserve the Senior Honors Thesis are given to the Special Collections Department of the Gingrich Library. I place no restrictions on this gift and hereby indicate this by signing below.

Title: Probing the Effects of Structural Variation on Concerted Proton-Electron Trasfer

Signature of Author: _____ Date: 5/4/2015

Printed Name of Author: Melissa Vetteson

Street Address: 839 Rupert Rd

City, State, Zip Code: Pottstown PA, 19464

Abstract

Concerted proton-electron transfer (CPET) involves the transfer of a proton and electron simultaneously to and from quantum mechanically distinct orbitals. Mechanistic clarification of CPET may be applicable to a variety of fields, such as the development of renewable energy resources. We are investigating base-appended radical cations; these organic systems are designed to undergo bidirectional CPET, with the proton-accepting and electron-accepting sites spatially separated. These systems allow us to model the relationship between structure and the kinetics and thermodynamics of CPET. Computational work reveals a kinetically unfavorable conformational change in the reaction of 10-(2-pyridinyl)-10*H*-phenothiazine radical cation (**PPT$^{\bullet+}$**) with 2,4,6-tri-*tert*-butylphenol. This conformational changed is believed to be responsible for the experimentally higher activation barrier relative to that for a similar molecule, 10-methyl-3-(2-pyridinyl)-10*H*-phenothiazine radical cation (**MPTP$^{\bullet+}$**) with the same donor. Hence, the conformational change affects the intrinsic barrier for CPET, in parallel to the same effect observed in electron transfer. We hypothesized that altering the size of the central ring will change the conformations of the radical cation and product. Current work is focused on 3,6-dimethoxy-9-(2-pyridinyl)-9*H*-carbazole radical cation (**PMC$^{\bullet+}$**), in which a five-atom ring replaces the central six-atom ring of the phenothiazine of **PPT$^{\bullet+}$**, and 5-(2-pyridinyl)-10,11-dihydro-5*H*-dibenzo[b,f]azepine radical cation (**PIB$^{\bullet+}$**), in which a seven-membered ring replaces the six-atom ring. Calculations indicate that these alterations eliminate the conformational change, and indicate that the intrinsic barrier will be lower for CPET with relative to that for **PPT$^{\bullet+}$/H^{+}**.

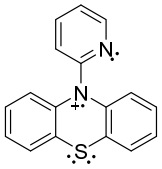

PPT$^{\bullet+}$

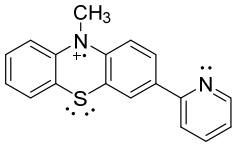

MPT$^{\bullet+}$

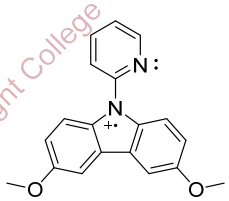

PMC$^{\bullet+}$

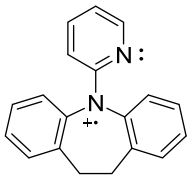

PIB$^{\bullet+}$

Table of Contents

Introduction and Previous Work

Part I: Proton Coupled Electron Transfer (PCET), Hydrogens Atom Transfer (HAT) and Concerted Proton-Electron Transfer (CPET)

Composed of a single electron and a single proton, hydrogen is the simplest element. Yet, it is one of the key drivers to some of the most essential chemical and biological processes.[1] The transfer of a hydrogen atom, or a proton and an electron, may occur by either a stepwise or concerted mechanism. The simultaneous transfer of a proton and an electron, proton-coupled electron transfer (PCET), plays an integral role in energy conversion processes such as photosynthesis and cellular respiration.[1] The elucidation of the elementary principles of PCET is crucial to understanding these processes, which may play a key role in the development of alternative renewable energy sources (e.g. artificial photosynthesis, H_2 storage and transfer).[2]

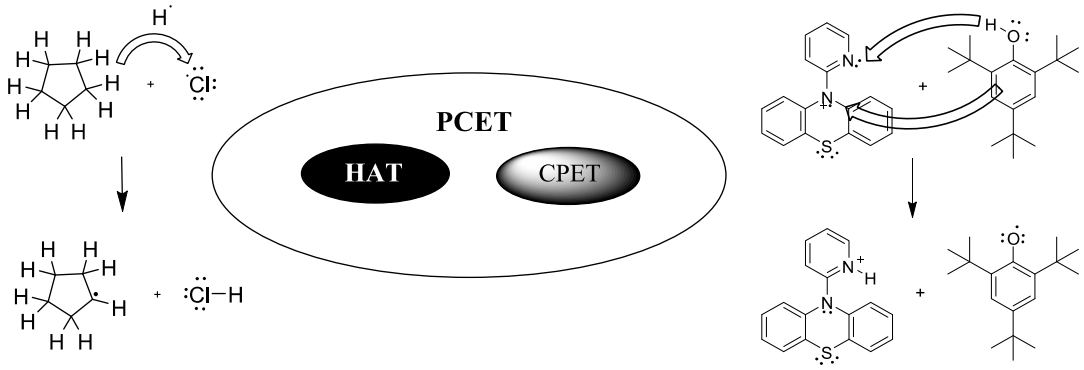

Figure 1. Proton-coupled electron transfer may refer to the concerted transfer of a proton and an electron. There are two subdivisions that are distinguished mechanistically. In hydrogen atom transfer (HAT), the proton and the electron transfer as a package; in concerted proton electron transfer they travel between quantum mechanically distinct orbital systems.

Proton coupled electron transfer (PCET) can be subdivided into two categories, hydrogen atom transfer (HAT) and concerted proton electron transfer (CPET), the latter being the subject of this senior thesis (see Figure 1). In HAT, the proton and electron transfer together as a package to the same site; CPET is distinguished by the fact the proton and electron are transferred to and from quantum mechanically distinct orbital systems.[3] Concerted proton-electron transfer has only been recognized in

the past 20 years, and has been primarily studied in inorganic systems. Clarifying the fundamental principles of CPET in simple organic systems is the motivation for the investigation of base appended radical cations. These organic systems are designed to undergo CPET (see Abstract). The proton is transferred from the σ system (to the lone pair on the pyridine), while the electron is transferred to the π system of the radical cation (see Figures 1 and 2).[4]

Concerted proton-electron transfer is an interesting reaction as it is mechanistically unique in comparison to other proton-electron transfer reactions. While HAT is electronically adiabatic, meaning the transfer occurs on a single energy surface, CPET is a non-adiabatic reaction involving a transfer from the reactant energy surface to the product energy surface.[4] Non-adiabatic processes are associated with a virtually instantaneous change in the electron charge distribution of the ground state between the reactant and the product potential energy surfaces (i.e., surface hopping).[1] Because the proton and electron are from different bonds and physically separated, a weak coupling between reactant and product state is often involved.[5] In our systems, a hydrogen bond pre-association is typical.

In CPET, there is a strong thermodynamic coupling between the proton and the electron.[6] Mixing of electronic and proton vibrational states across more than one potential energy surface leads to a single quantum mechanical event, the particles change quantum states simultaneously.2[7] One may state that the proton tunnels through the two wells formed by the interacting electronic states.[7] The proton's motion is treated as an additional quantum mode in an otherwise standard electron transfer system.[7] The degree of non-adiabaticity is connected to the extent of charge distribution in a PCET process; a large distribution of charge corresponds to a non-adiabatic process.[8]

Typically, thermodynamics do not influence kinetics, and there is no relationship between $\Delta G°$ and $\Delta G^{‡}$ (activation free energy).[9] One exception to this rule occurs in reactions between solvated donors and acceptors that exchange electrons.[9] In such cases, Marcus theory may be used to predict the rate constants of a system based off of thermodynamic parameters. To verify which process is occurring, the Gibbs free energy ($\Delta G°$) of intermediates and activation free energies of reaction ($\Delta G^{‡}$) are compared. Compounds proceed from reactant to product along a minimal energy path. If the $\Delta G^{‡}$ is significantly less than the $\Delta G°$ of any intermediates, the mechanism is considered to be concerted. Even if the energy of the intermediate is only slightly lower than that of the concerted transition state (TS), CPET will still be the dominant mechanism.[3]

Part 2: Experimental Mechanistic Determination and Hypothesis

Our laboratory has synthesized and investigated the mechanism for the reaction of **PPT$^{\bullet+}$** and **MPTP$^{\bullet+}$** with hindered phenols (Figure 2). Three mechanisms were considered: (a) proton transfer-electron transfer, with a dicationic intermediate (PT-ET); (b) electron transfer-proton transfer with a neutral intermediate (ET-PT); and (c) CPET, with no intermediate. In each case, the barrier of reaction derived from rate constant data was lower than the free energy for intermediates, calculated through electrochemistry and acid-base titration data (Table 1), and hence the reactions undergo CPET.[3]

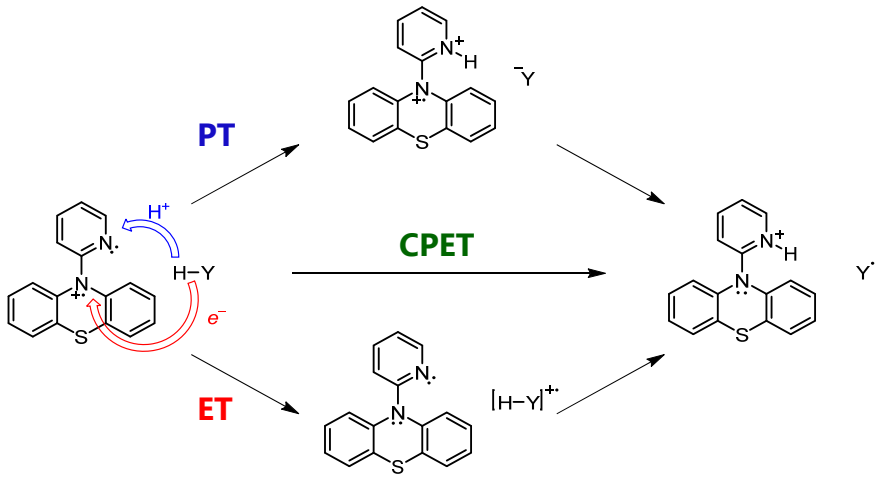

Figure 2. Possible pathways for net hydrogen atom transfer for base-appended radical cations.1

Table 1. Data for reactions of radical cations and hindered phenols.[3]

system	ΔG_{ET}	ΔG_{PT}	$\Delta G^{\ddagger}$
PPT$^{\bullet+}$+^{t}Bu$_3$ArOH	18.2	29.9	15.9
MPTP$^{\bullet+}$+^{t}Bu$_3$ArOH	19.8	26.4	13.4

In the process of the mechanistic determination, the bond dissociation free energies (BDFE) were determined. The BDFE is a measure of bond strength for the product (**PPTH$^+$**, for example), and radical cation corresponding to a product with a large BDFE abstract hydrogens from stronger X–H bonds. To derive a formula for the BDFE, pK_a values are converted to free energies with equation 1, and reduction potentials are converted to free energies with equation 2. The BDFE formula for **PPTH$^+$** → **PPT$^{\bullet+}$ + H$^\bullet$** is based off of Hess's law and the square scheme, yielding equation 3.[6] The overall formula for reaction with an acceptor is equation 4, derived with Hess's law.

$$\Delta G° = -RT \ln K \quad (1)$$

$$\Delta G° = -nFE \quad (2)$$

$$\text{BDFE(kcal/mol)} = 1.37pK_a + 23.06E + 54.9 \quad (3)$$

$$\Delta G° = \text{BDFE (donor)} - \text{BDFE (acceptor)} \quad (4)$$

When corrected for driving force, **MPTP$^{\bullet+}$** reacts significantly faster than **PPT$^{\bullet+}$**, even after accounting for differences in driving force. For example, in reaction with 2,4,6-tri-*tert*-butylphenol, **PPT$^{\bullet+}$** has a barrier of reaction that is 2.5± 1.4 kcal/mol higher than that for **MPTP$^{\bullet+}$** despite being 0.7 ± 0.1 kcal/mol downhill.[3] Calculations performed over the summer of 2011 indicate that **PPT$^{\bullet+}$** undergoes a conformational change during the reaction (Figure 3). In the radical cation precursor, the phenothiazine ring is planar, and the pyridyl ring is orthogonal to it. During the reaction, the nitrogen and sulfur change hybridization from sp^2 in the radical cation to sp^3 in the product. In the product, the phenothiazine ring adopts a pseudo-boat conformation with the pyridinium in the pseudo-axial position and rotated 90° from its position in the radical cation (see Figure3 below). Steric hindrance between the hydrogens in the 1 and 9 positions of the phenothiazine ring and the 3' position of the pyridine allow for the high barrier.[3] In contrast, calculations indicate that the entire **MPTP$^{\bullet+}$** molecule remains planar throughout the reaction with minimal steric hindrance and hence occurs with a significantly lower barrier.[3]

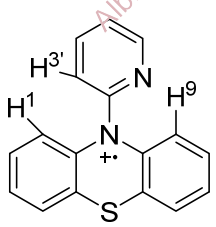

PPT$^{\bullet+}$

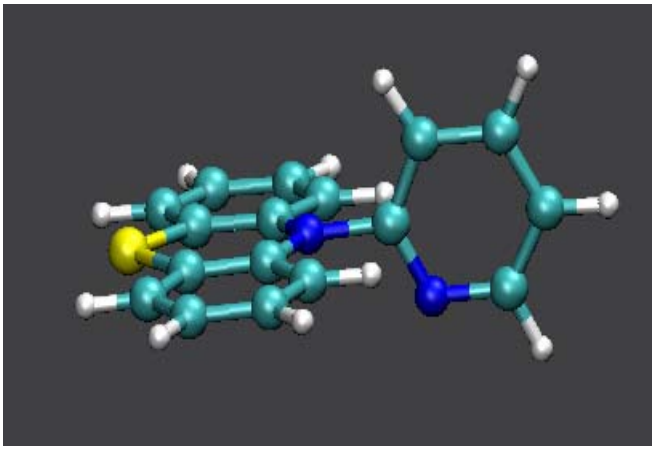

PPTH^{+}

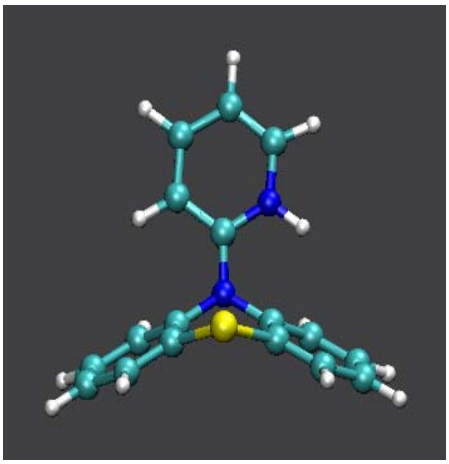

Figure 3. In **PPT$^{\bullet+}$,** the phenothiazine ring is planar, and orthogonal to the pyridine ring. In PPTH^{+}, the phenothiazine ring is now bent with a pyramidalized N and S. The pyridine is now pseudo-axial and rotated away from the N-S axis.

To further test these conformational effects, we proposed two geometric alterations to the central ring system of the phenothiazine. The five-atom central ring of **PMC$^{\bullet+}$** is proposed to minimize the hydrogen-pyridine interactions, while the seven-membered central ring of **PIB$^{\bullet+}$** is proposed to maximize the hydrogen-pyridine interactions. To the extent that these changes prevent a conformational change, both molecules could have a lower intrinsic barrier than **PPT$^{\bullet+}$**.

Results and Discussion

PMC$^{\bullet+}$/H^{+}

Initial calculations on **PMC$^{\bullet+}$** and **PMCH^{+}** indicate a planar phenothiazine in both molecules (Figure 4). Contraction of the central ring from six to five atoms allows the molecule to remain in this conformation; the sulfur is no longer present to act as a hinge. Steric interactions between hydrogens in the 1 and 8 positions and the pyridine ring also appear less problematic than in **PPT$^{\bullet+}$**. Molecular orbital calculations suggest the radical character is spread across the lower ring system, similar to **PPT$^{\bullet+}$** (Figure 5).

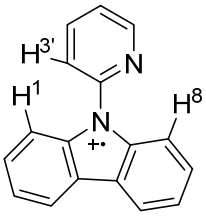

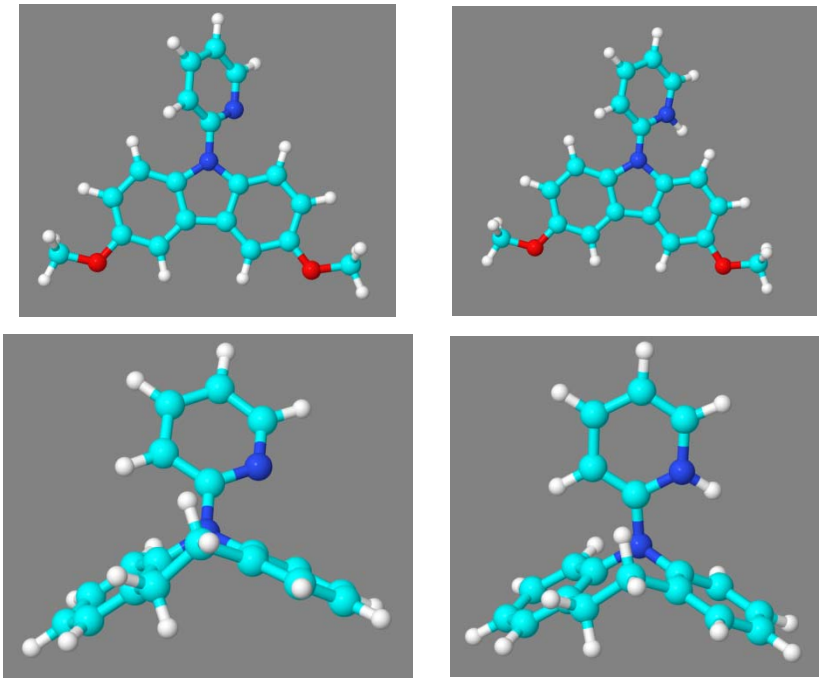

Figure 4. The radical cations (top) and protonated products (bottom) for **PMC$^{\bullet+}$/PMCH^{+}** (left) and **PIB$^{\bullet+}$/PIBH^{+}** (right). Employing MO6-2x/6-31+g(d,p) in vacuo, preliminary calculations indicate that the phenothiazine ring of **PMC$^{\bullet+}$** and **PMCH^{+}** is planar (like **PPT$^{\bullet+}$**) and does not undergo a conformational change. The phenothiazine ring of **PIB$^{\bullet+}$** and **PIBH^{+}** is bent (like **PPTH^{+}**).

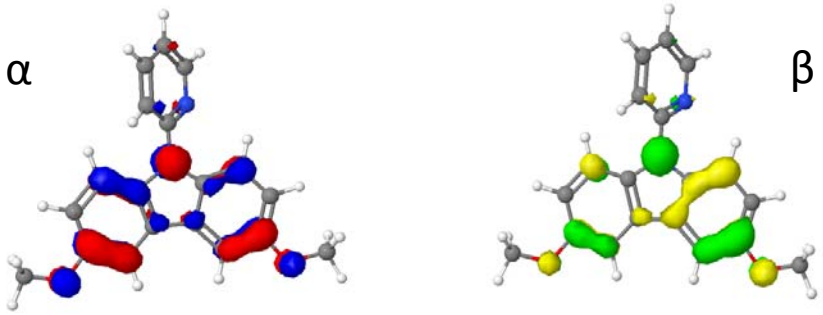

Figure 5. Molecular orbital calculation of the SOMO of **PMC$^{\bullet+}$** show the radical character to be isolated on the carbazole.

A possible transition state for the reaction of 2,4,6-tri-*tert*-butylphenol has also been isolated (Figure 6). Geometrically, it is consistent with other systems we have modeled (Table 2). Typical hydroxyl (O-H) bond length is 0.98 Å while typical amine (N-H) bond length is 1.05 Å. The hydrogen and the oxygen distance (1.12 Å) and the hydrogen-nitrogen distance (1.38 Å) verify that the proton is in transfer, and bound to neither. Linearity of the bond angle (162.5°) supports a hydrogen bond pre-association. This geometric trend was noted in previous work,[3] and further substantiates our claim of transferability; once we have isolated a transition state for a particular donor it may be used as a starting point when modeling that donor with other acceptors.

Table 2. Geometric parameters for transition states between radial cations and 2,4,6-tri-*tert*-butylphenol.

Acceptor	r (N-H), Å	r (O-H), Å	r (O-N), Å	a (O-H-N), °
PPT$^{\bullet+}$	1.393	1.112	2.478	163.0
MPTP$^{\bullet+}$	1.385	1.119	2.488	166.7
PMC$^{\bullet+}$	1.38	1.12	2.474	162.5

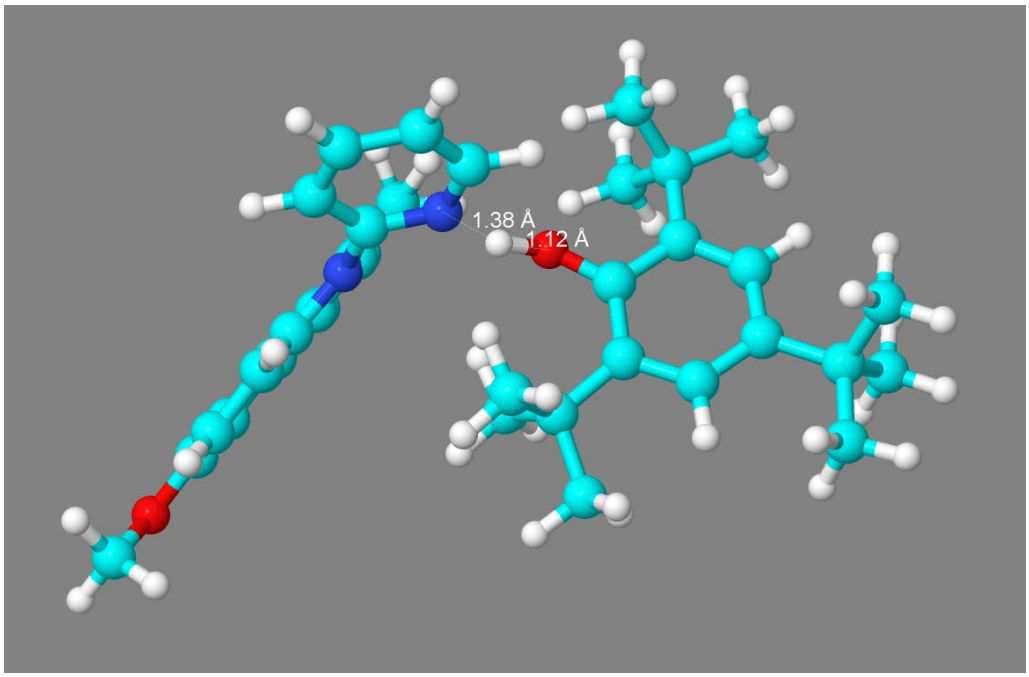

Figure 6. Transition state for reaction of **PMC$^{\bullet+}$** and 2,4,6-tri-*tert*-butylphenol.

Experimental wet chemistry was also performed. Synthesis of the 3,6-dimethoxy-9*H*-carbazole was executed using via a copper(I) iodide-catalyzed nucleophilic aromatic substitution. Other methods of synthesis were attempted with poor results. The product was confirmed via ^{1}H NMR (Figure A1) before proceeding to the next step, generation of the neutral radical cation precursor. This was achieved by Buchwald-Hartwig amination. The pale tan crystalline **PMC** product was collected in a 69% yield. The product was again confirmed by ^{1}H NMR (Figure A2) and infrared spectroscopies (Figure A3).

Cyclic voltammetry was performed on the radical cation precursor. This determines whether the radical cation is stable on an electrochemical timescale and provides the reduction potential for the radical cation-neutral couple (**PMC$^{\bullet+/0}$**). From the cyclic voltammogram, a reduction potential of 0.64 V vs. $Cp_2Fe^{+/0}$ was determined. This significantly larger than that for either **MPTP$^{\bullet+/0}$** or **PPT$^{\bullet+/0}$**, due to the lack of the electron donating sulfur. (The parallel compound with the unsubstituted carbazole had an even high potential with an irreversible cyclic voltammogram due to dimerization.)

The pK_a of **PMCH$^+$** was determined to evaluate the basicity of the **PMC**. Addition of **PMC** to thymol blue in a titration resulted in the deprotonation of the indicator which was monitored by absorbance in the UV-vis spectrum. The concentration of the deprotonated thymol blue species was plotted versus the concentration of the **PMC**. Hess's law, Beer's law, and mass balance were then used

to determine the pK_a from the calculated equilibrium constant (see Experimental). **PMC** is slightly less basic (pK_a of **PMCH**$^+$ = 9.9) than either **PPT** or **MPTP** (10.9 and 11.1 and respectively). This may be connected to the accessibility of the basic site or to a slightly more electron deficient pyridine ring.

The above thermochemical data may be combined to evaluate the molecules bond dissociation free energy (BDFE) for **PMCH**$^+$ → **PMC**$^{\bullet+}$ + H$^\bullet$ using equation 3. This will allow us to determine the $\Delta G°$ for reaction with a hydrogen atom donor (**PMC**$^{\bullet+}$ + HA → **PMCH**$^+$ + A$^\bullet$) using equation 4. The BDFE of **PMCH**$^+$ was calculated to be 83.3 kcal/mol, which is much higher than either **PPTH**$^+$ (78.8 kcal/mol) or **MPTPH**$^+$ (77.5 kcal/mol); the increase in BDFE is due to the increased in reduction potential. A graph with these data and that for other compounds is represented on Figure 7.

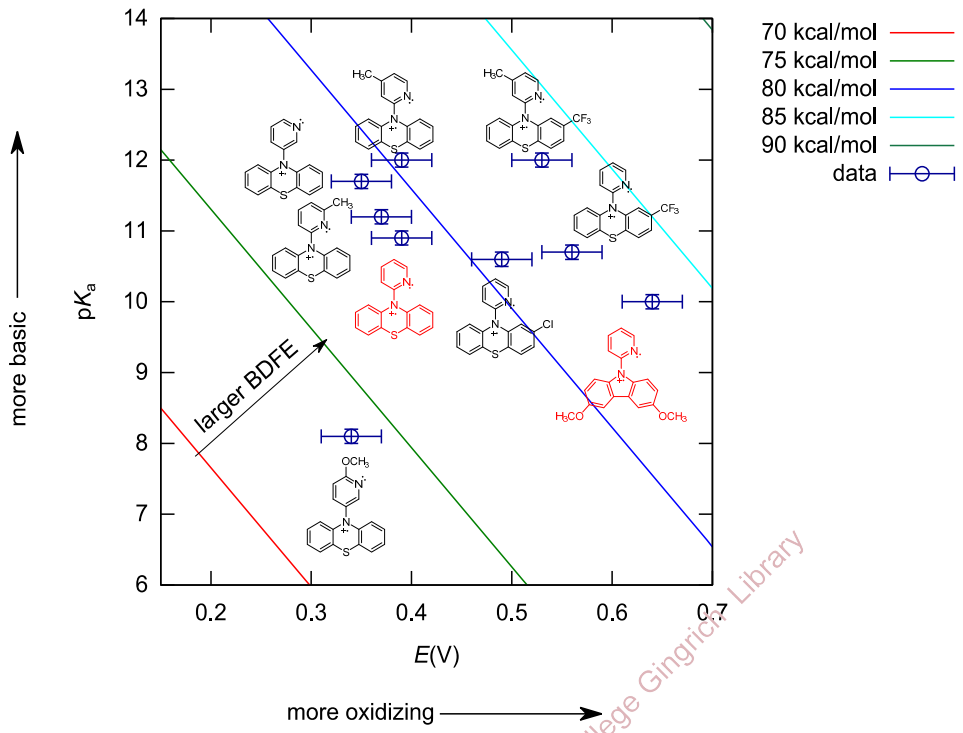

Figure 7. Graph indicating the relationship of pK_a, E and BDFE for several base-appended radical cations. Data from refs 3 and 10.

While calculations on **PPT**$^{\bullet+}$**/H**$^+$, **MPT**$^{\bullet+}$**/H**$^+$ and related systems have close experimental and computational values for the BDFE, the values for **PMC**$^{\bullet+}$**/H**$^+$ (83.3 and 68.7) are not close (see table 3). One possibility for the discrepancy may be that the molecules are not in the lowest energy conformation. The calculations are currently being repeated with the methoxy groups rotated away

from the ring as well as staggered to see if these yield BDFEs more consistent with the experimental evidence. Further rotation of the appended pyridine will also be explored; it is currently not orthogonal to the phenothiazine ring. Neither alteration should affect the planarity of the phenothiazine ring.

Upon convergence of the optimization and vibrational frequency analysis being performed on the **PMC$^{\bullet+}$** and **PMCH^{+}** with the rotated methoxy groups, the free energies will be compared and the BDFE calculated. A new transition state calculation will be performed, followed by an intrinsic reaction coordinate analysis in both the forward and backwards direction to establish the program has indeed converged on the correct transition state. The free energy of the transition state will allow for the $\Delta G^{\ddagger}$ to be predicted. Molecular orbital calculations will also be performed. Experimentally, the radical cation needs to generate and analyzed by UV-vis spectroscopy and the kinetics with hinderer phenols determined.

PIB$^{\bullet+}$/H^{+}

The compound with a seven-atom ring also was predicted to have a higher BDFE and a lower intrinsic barrier than those for **PPT$^{\bullet+}$/H^{+}**. Although the ring size allows for increased flexibility, it may also allow for increased steric interactions; nonetheless, no conformational change is expected. Loss of aromaticity in the lower ring system should lead to a less delocalized unpaired spin, and hence a less stable and reactive radical cation species with a higher reduction potential than **PPT$^{\bullet+}$**.

Calculations were performed on the radical cation reactant (**PIB$^{\bullet+}$**) and the cationic product (**PIBH^{+}**) using methods described previously. Optimization and vibrational frequency analysis indicate both structures have the pseudo-chair phenothiazine with the pyridine pseudo-axial, similar to the **PPTH^{+}** (see Figure 4). This alleviates the steric pressure between the between the 4 and 6 hydrogens of the lower iminodibenzyl and the pyridine ring. The BDFE was predicted computationally to be 92.2 kcal/mol, allowing for net hydrogen abstraction reactions that will be much more downhill than any of the other radical cations. The position of the pyridine ring makes the proton accepting site readily available. This may lend to an increased basicity, which combined with the more reactive radical site, would yield a larger BDFE.

The synthesis of the radical cation precursor **PIB** was attempted with the Buchwald-Hartwig amination, and a crude product was isolated. The initial ^{1}H NMR (Figure A4) indicates some product may be present, but the spectrum and TLC suggest a large amount of starting material remains. After an appropriate solvent is determined a column will be run. Once purified, the above stated thermochemical data will be gathered to determine an experimental BDFE. There is a concern that the

molecule will dimerize when the cyclic voltammetry is performed in parallel with the unsubstituted carbazole system; similar functionalization with methoxy groups may be necessary. Computationally, molecular orbital calculations will be run. An optimization and vibrational frequency determination on the transition state with 2,4,6-tri-*tert*-butylphenol will follow, which will allow for the calculation of a predicted $\Delta G^{\ddagger}$.

Conclusion

The thermodynamic parameters for the molecules described are provided in Table 3. Both the **PMCH**$^{+}$ and the **PIBH**$^{+}$ appear to have a larger BDFE than **PPTH**$^{+}$, meaning they should be capable of breaking stronger bonds. The conformations of **PMC**$^{\bullet+}$ and **PMCH**$^{+}$ appear to mimic that of **PPT**$^{\bullet+}$ while the **PIB**$^{\bullet+}$ and the conformations of **PIBH**$^{+}$ resembles that of **PPTH**$^{+}$. Kinetics experiments and computation of the transition state will allow us to determine if these two molecules indeed have a lower intrinsic barrier. This data will provide insight as to whether or not the conformational change is correlated to the higher intrinsic barrier observed in **PPT**$^{\bullet+}$.

Table 3. Thermodynamic summary or **PPT**, **MPTP**, **PMC**, and **PIB**. The reduction potentials are in V and the free energies are in kcal/mol.

	E (V)[a]	pK_a[b]	BDFE exptl[b]	BDFE comptl[b]	$\Delta G^{\ddagger}$ exptl[c]	$\Delta G^{\ddagger}$ comptl[c]	$\Delta G°$ exptl[c]	$\Delta G°$ comptl[c]
PPT	0.39	10.9	78.8	76.0	15.9	12.9	–1.7	1.13
MPTP	0.32	11.1	77.5	71.8	13.4	8.7	–0.4	5.32
PMC	0.64	9.9	83.3	68.7	-	-	–6.5	8.43
PIB	-	-	-	92.2	-	-	-	–15.13

[a]The value for E is for the radical cation-neutral couple in 0.1 M Bu_4NPF_6 in MeCN and referenced for $Cp_2Fe^{+/0}$. [b]For the protonated compound. [c]Values for $\Delta G^{\ddagger}$ and $\Delta G°$ correspond to the reaction between the radical cation and 2,4,6-tri-*tert*-butylphenol.

Methods

Computational (DFT):

Transition states that may not be isolated experimentally are accessible computationally. In order to theoretically describe these reactions the proton and the electron must be considered quantum mechanically (as waves).[11] High-level quantum computations can offer insight towards understanding organic systems.[4] Total molecular wave function depends on the positions of all the nuclei and

electrons. Electrons are lighter, thus can move more rapidly and instantly respond to any changes in the relative position of the nuclei. This allows for the wave function to be separated into two parts, the electronic and nuclear. If the nuclear is held fixed, one only has to solve the electronic wave function. A potential energy surface (PES) is created by determining the electronic energy of a molecule, and then varying the positions of the nuclei.[5]

WebMO was the interface employed to run the Gaussian 09 computational chemistry software on 24 processors. Solving the Schrödinger equation would provide the wave function, and thus a complete description of the molecule. Unfortunately this may only be done for the hydrogen atom. The program instead "fakes" a solution to the Schrodinger equation via density functional theory (DFT). Schrödinger wave function gives one the probability of all the electrons in a system individually. Density functional theory solves a simpler problem, the total probability density of all the electrons collectively. Computationally more efficient, DFT provides an exact theory with an approximate solution.[5]

When using DFT, an exchange correlation functional, or model chemistry (such as B972) must be specified. This model chemistry deals with the physics of how electrons behave. An exchange correlation functional is the sum of two components. The exchange functional deals with the attraction of the electrons of one atom to the nucleus of another, while the correlation functional deals with the electron- electron repulsions between the molecules.[5]

Next a basis set is selected. A basis set is a description of a probability function in space relative to the nucleus. A minimum basis set has one basis function for every formally or partially occupied orbital (single zeta).[5] The minimum is usually inadequate, and may be doubled, or tripled. The process is analogous to the calculus method of estimating area under a curve. A larger basis set provides a better approximation. As most chemistry focuses on the valence electrons, split basis sets were developed (single zeta core, double or triple valence), a dash signifies the separation between the core and valence (ex: 6-31G)[12] basis set.

The transition state geometries and thermochemistry are dependent on non-bonded interactions between the hydrogen acceptor and hydrogen donor. Accurate modeling of non-covalent charge transfer complexes is a challenge in density functional theory .[13] The B972 functional was shown to be accurate for thermochemical quantities (reaction energies, ionization potentials, etc.) but was not adequate to accurately model non-bonded interactions. Research has indicated the M06-2x functional provides the best performance for the study of non-covalent interactions.[13] It accurately the models transition states of such non-bonded exchanges, and the results of hydrogen transfer barrier height calculations are considered superior.[13] It is highly recommended for the study of main-group chemistry,

and is also known to provide accurate thermochemical and kinetic data.[13] This model chemistry was employed for all future calculations.

Experimental

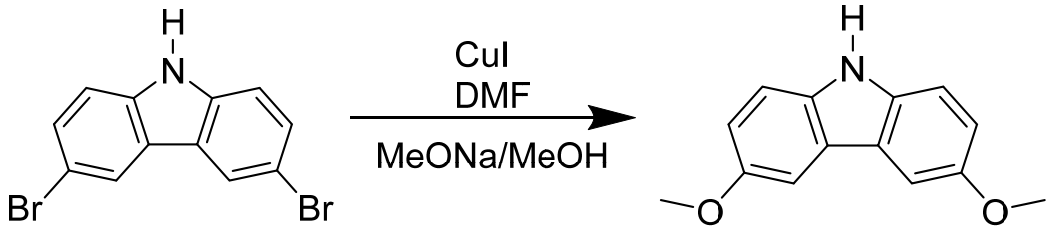

Copper (I) iodide catalyzed nucleophilic aromatic substitution. [14] Sodium methoxide (3.5 mL) was added to a round bottom flask under N_2 along with 1.001 g 3,6-dibromo-9*H*-carbazole, 1.170 g copper iodide, and 1 mL DMF. The reaction was left to reflux for 24 h. More DMF was added the following morning. After the reaction refluxed for an additional 24 h, the reaction was cooled and filtered through SiO_2 and washed with ethyl acetate. The solvent was removed under reduced pressure. The crude product was purified via silica gel chromatography using hexanes/CH_2Cl_2 (6/4 v/v to 1/1 v/v to CH_2Cl_2) in 1 L portions. Removal of solvent resulted in a solid. ^{1}H NMR (400 MHz, $CDCl_3$) δ 3.9 (s, 6H), 7.1(d, 2H), 7.3 (d, 2H), 7.5 (s, 2H), 7.8 (br s, 1H, NH) ppm; mp 103-105 °C.

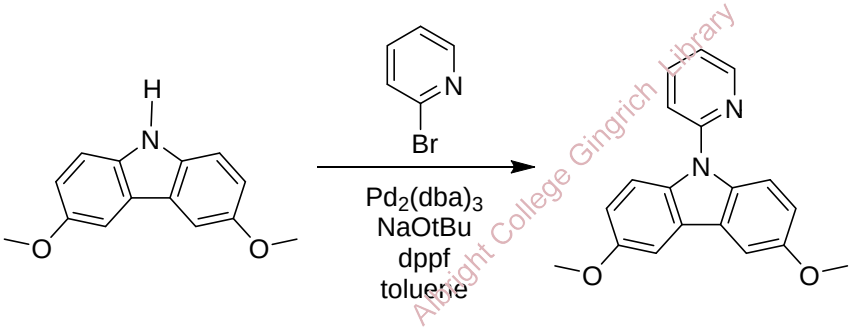

Buchwald-Hartwig amination to yield PMC.[15] In a round bottom flask, 0.5340 g of 3,6-dimethoxy-9*H*-carbazole was added to 25 mL of dry toluene flask along with 0.3637 g of sodium *t*-butoxide, 0.0084 g 1,1'-bis(diphenylphosphino)ferrocene, 0.0105 g $Pd_2(dba)_3$, and 0.26 mL 2-bromopyridine. After the reaction refluxed for 24 h, additional catalyst and ligand were added. After 3 days, identical amounts of catalyst and ligand as well as an additional portion of 2-bromopyridine were added. The reaction was refluxed for an additional day. After cooling, the mixture was filtered over a silica plug and washed with

50/50 v/v toluene/ethyl acetate. After rotary evaporation, the remaining product was a yellow-brown solid. The crude was crystallized in 16/1 v/v mixture hexanes/ethyl acetate to produce fine, tan crystals that were gathered by vacuum filtration at a 69% yield. The product was verified by ^{1}H NMR spectroscopy. ^{1}H NMR (400 MHz, $CDCl_3$) δ 3.95 (s, 6H), 7.1(d, 2H), 7.25 (m, 1H), 7.5 (s, 2H), 7.6 (d, 2H), 7.8 (d, 2H), 7.9 (t, 1H), 8.7 (t, 1H); mp 103-105°C

Buchwald-Hartwig amination. [13]

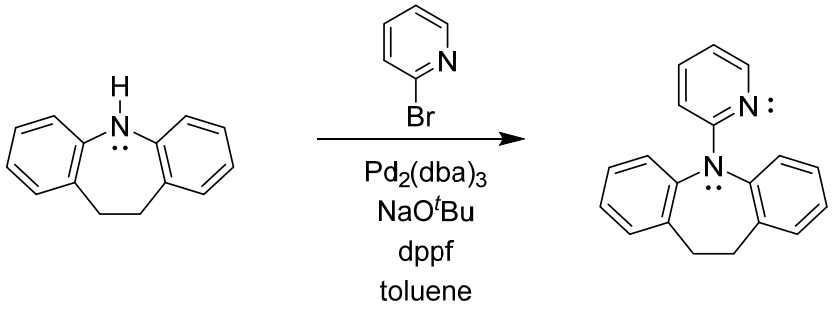

Buchwald-Hartwig amination to yield PIB.[13] In a round bottom flask, 1.758 g of iminodibenzyl was added to 25 mL of dry toluene flask along with 1.3943 g of sodium *tert*-butoxide, 0.0364 g 1,1'-bis(diphenylphosphino)ferrocene, 0.0445 g $Pd_2(dba)_3$, and 1 mL 2-bromopyridine. After the reaction refluxed for 24 h, additional catalyst and ligand were added (0.033 g dppf/0.0453 g $Pd_2(dba)_3$) . After another 24 h, identical amounts of catalyst and ligand as well as an additional 0.2 mL of 2-bromopyridine were added. The reaction was refluxed for an additional day. After cooling, the mixture was filtered over a silica plug and washed with 50/50 v/v toluene/ethyl acetate. After rotary evaporation, the remaining product was a dark brown solid. The crude product was inspected via ^{1}H NMR. Although the desired peaks appear to me present, it is believed there is still some starting material present. Future work includes purification via column chromatography. ^{1}H NMR (400 MHz, $CDCl_3$) δ 3.15(s, 2H), 3.16(s, 2H), 6.0 (s, 1H, NH), 6.4-7.6 (m).

Thermodynamic characterization of PMC

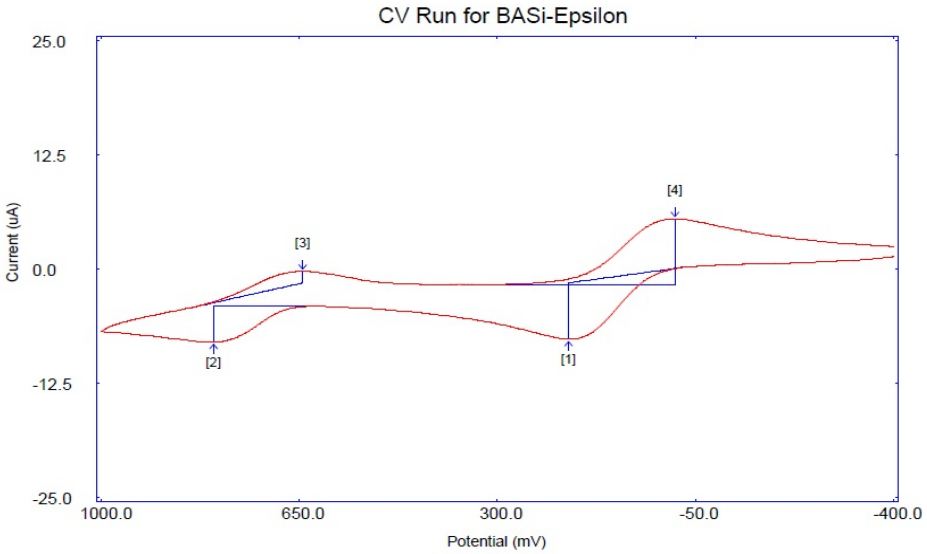

Cyclic Voltammetry. Cyclic voltammetry was performed in 0.1 M Bu_4NPF_6 in acetonitrile with a glassy carbon working electrode, $Ag/AgNO_3$ (0.01 M) reference electrode and a platinum wire auxiliary electrode. Ferrocene was added as an internal standard.

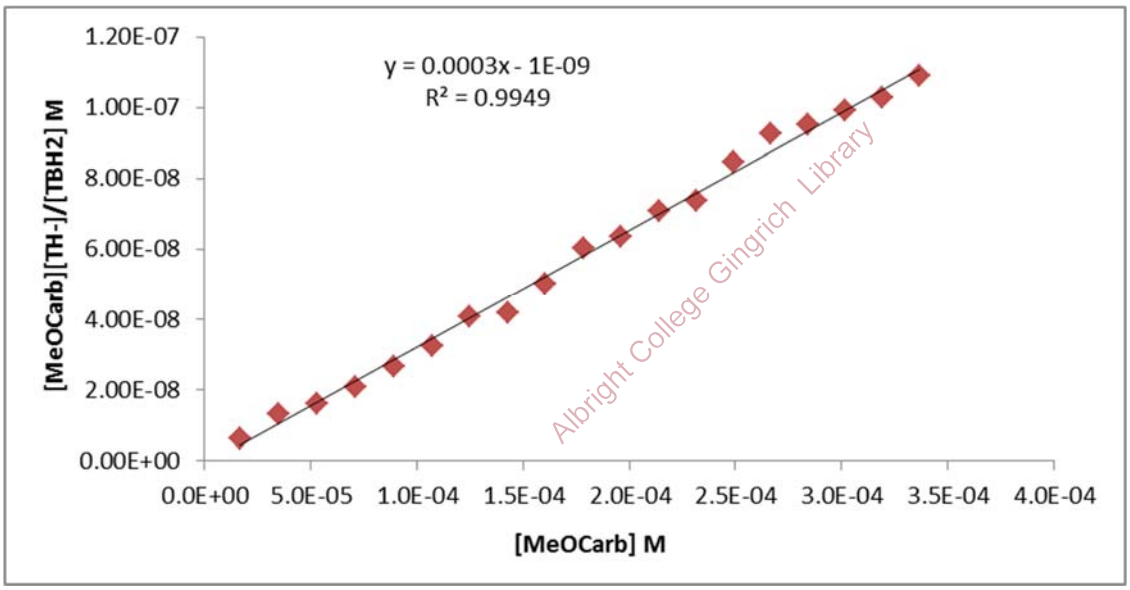

Acid-Base Equilibrium for pK_a determination.[3] The equilibrium constant for the radical cation precursors and thymol blue were determined by adding 50 µL aliquots of a 0.88 mM solution of the radical cation precursors to 3.0 mL of a 0.40 mM solution of thymol blue solution. The absorbance at

395 nm ($\varepsilon = 1.65 \times 10^4\ M^{-1}\ cm^{-1}$)[16] corresponding to an absorption of the deprotonated thymol blue (TH^-) was used to determine $[TH^-]$ after correcting for volume. Equations 6, 7, and 8 were used to account for mass balance. Slope of the line is equal to K_{eq}.

$$TH_2 + PMC \rightleftharpoons TH^- + PMCH^+$$

$$K_{eq} = \frac{[TH^-][PMCH^+]}{[TH_2][PMC]} \quad (5)$$

$$[TH_2] = [TH_2]_{initial} - [TH^-] \quad (6)$$

$$[PMC^+] = [TH^-] \quad (7)$$

$$[PMC] = [PMC]_{initial} - [TH^-] \quad (8)$$

The slope of a plot of $[PMCH^+][TH^-]/[TH_2]$ vs. [PMC] provided the equilibrium constant. The procedure for the other compounds was similar.

Appendix

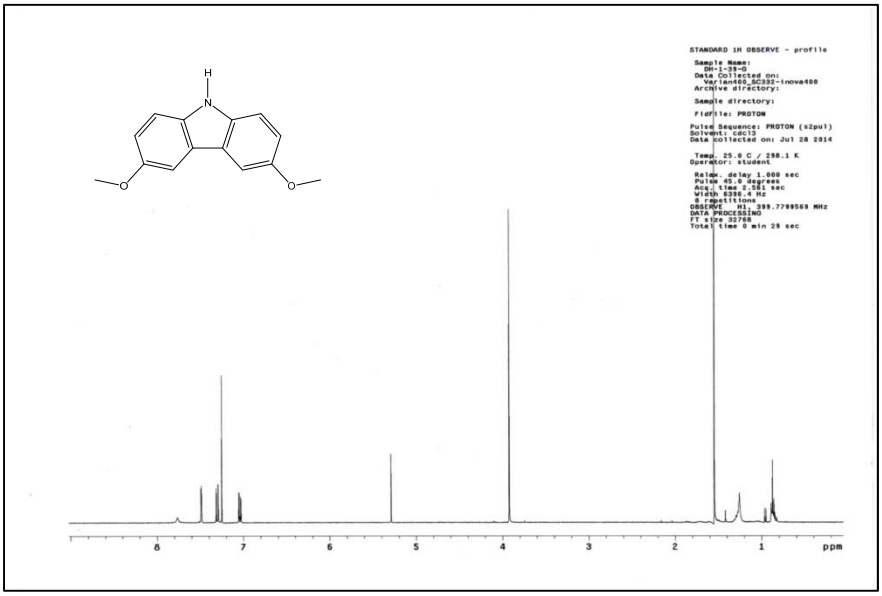

Figure A1. ^{1}H NMR of 3,6-dimethoxy-1*H*-carbazole synthesized via nucleophilic aromatic substitution. ^{1}H NMR (400 MHz, $CDCl_3$) δ 3.9 (s, 6H), 7.1(d, 2H), 7.3 (d, 2H), 7.5 (s, 2H), 7.8 (br s, 1H, NH); mp 103-105°C

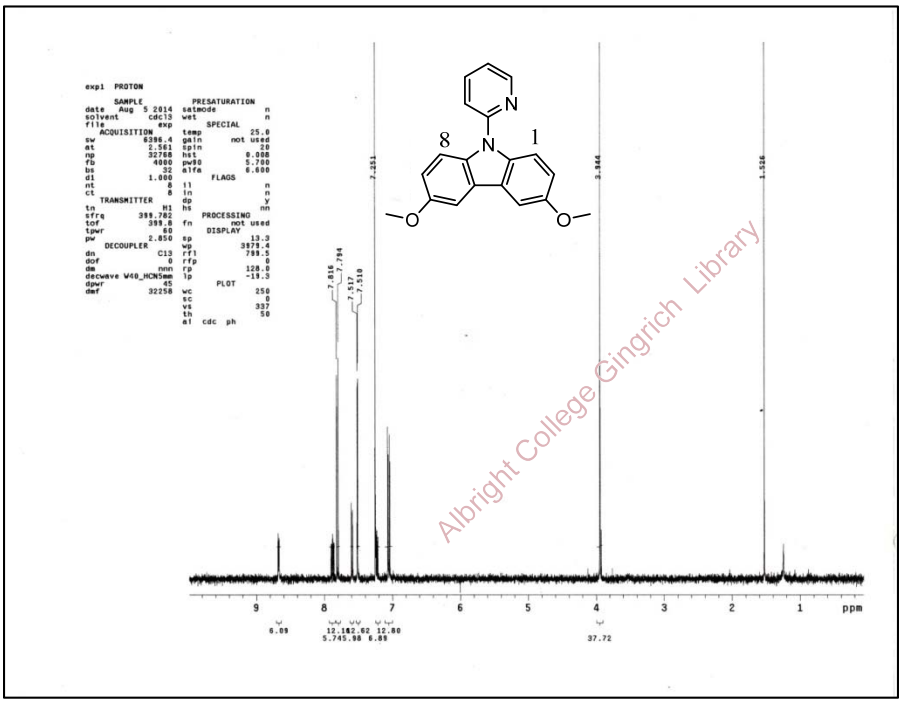

Figure A2. ^{1}H NMR of the **PMC** neutral radical cation precursor synthesized by Buchwald-Hartwig amination. ^{1}H NMR (400 MHz, $CDCl_3$) δ 3.95 (s, 6H), 7.1(d, 2H), 7.25 (m, 1H), 7.5 (s, 2H), 7.6 (d, 2H), 7.8 (d, 2H), 7.9 (t, 1H), 8.7 (t, 1H); mp 103-105°C.

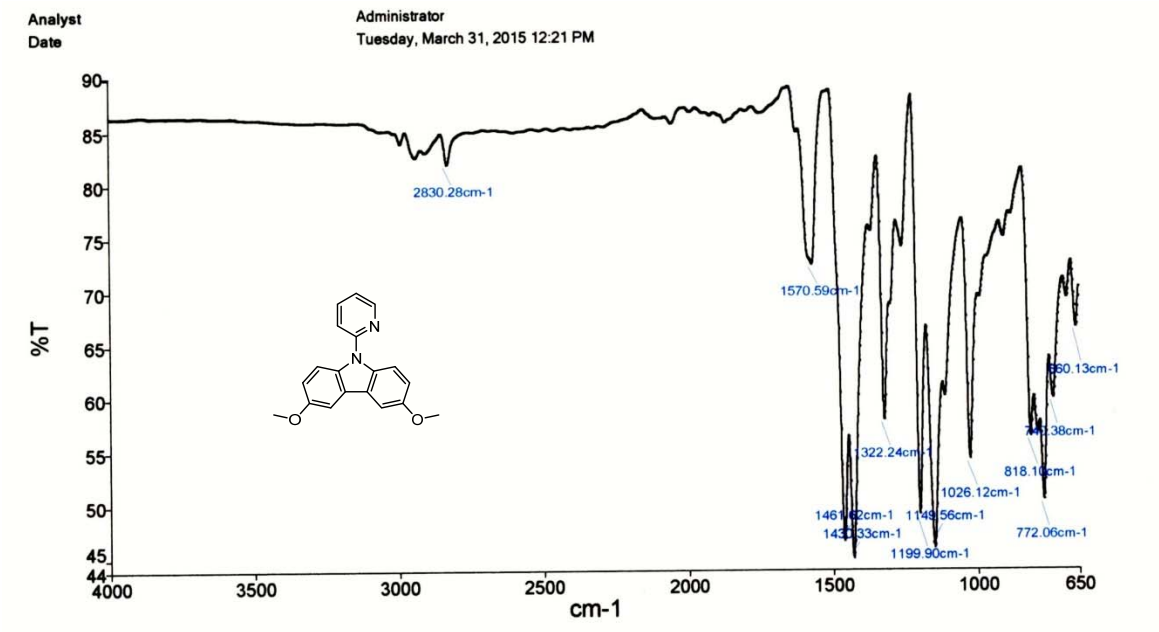

Figure A3. IR spectra of **PMC.** No undesirable functional groups are noted, but the C-H stretching region ~2800-3000 cm^{-1} supports the presence of an aromatic ring system.

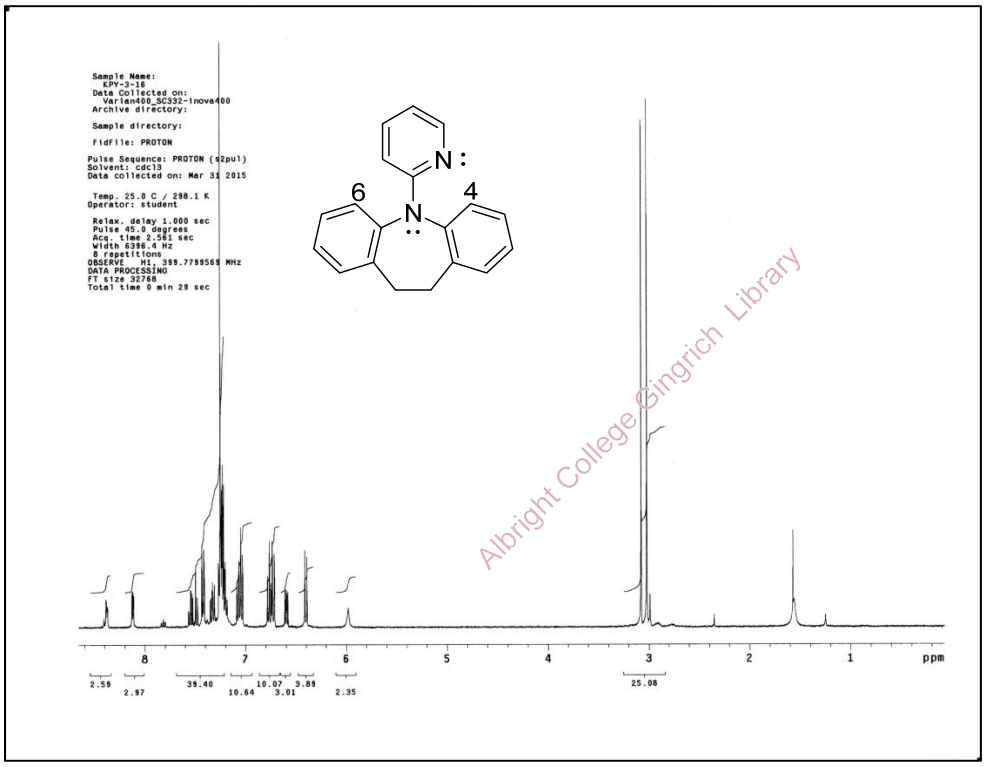

Figure A4. ^{1}H NMR of the crude **PIB** neutral radical cation precursor synthesized via Buchwald-Hartwig amination. ^{1}H NMR (400 MHz, $CDCl_3$) δ 3.15(s, 2H), 3.16(s, 2H), 6.0 (s, 1H, NH), 6.4-7.6 (m).

References

(1) Mayer, J. M. *Annu. Rev. Phys. Chem.* **2004**, 55, 363-390.

(2) Hammes-Schiffer, S. *Proc. Natl. Acad. Sci. USA* **2011**, 108, 21, 8531-8532.

(3) Welker, E. A.; Tiley, B. L.; Sasaran, C. M.; Zuchero, M. A.; Tong, W.-T.; Vettleson, M. J.; Richards, R. A.; Geruntho, J. G.; Stoll, S.; Wolbach, J. P.; Rhile, I. J. In preparation.

(4) Weinberg, D. R; Gagliardi, C.J.; Hull J.F.; Murphy C.F.; Kent C.A.; Westlake, B.C.; Paul, A.; Ess, D.H.; McCafferty, D.G.; Meyer, T.J. *Chem. Rev.* **2012,** *112,* 4016-4093.

(5) Bachrach, S. M., *Computational Organic Chemistry;* Wiley: NJ, 2007; pp 1-32.

(6) Warren J. J.; Tronic, T. A; Mayer, J. M. *Chem. Rev*. **2010,** *110,* 6961-7001.

(7) Georgievskii, Y., Stuchebrukhov, A. A. *J. Chem. Phys.* **2000**, 113, 23, 10438-10450.

(8) Schrauben, J., Cattaneo, M., Day, T., Tenderholt, A., Mayer, M. *J. Amer. Chem. Soc.,* **2012,** 134, 16635-16645.

(9) Silverstein, T. *J. Chem. Educ.* **2012**, 89, 1159-1167.

(10) Simpson, F. M. C.; Robinson, D. R.; Welker, E. A.; Rhile, I.J. Unpublished work.

(11) El Ghachtouli, S.; Lassalle-Kaiser, B.; Dorlet, P.; Guillot, R.; Anxolabehere-Mallart, E.; Costentin, C.; Aukauloo, A., *Energy Environ. Sci*. **2011**, 4(6), 2041-2044

(12) Mayer, J. M.; Hrovat, D.A.; Thomas, J.L.; Borden, W.T. *J. Am. Chem. Soc.* **2002**, *124*, 11142-7.

(13) Zhao, Y.; Truhlar, D. G. *Theor. Chem. Account* **2008,** *120,* 215-241.

(14) Benoit Liegauly, D.L., Huestis, M.P., Stuart, D.R., Fagnou, K. *J. Org. Chem.* **2008**, 73, 5022-8.

(15) (a) Driver, M. S.; Hartwig, J. F. *J. Am. Chem. Soc.*, **1996,** 118*,* 7217-7218. (b) Franz, A. W.; Popa, L. N.; Frank Rominger, F.; Müller, T. J. J. *Org. Biomol. Chem.* **2009,** *7*, 469-475.

(16) Kolthoff, I. M.; Chantooni, M. K., Jr.; Bhowmik, S. *Anal. Chem.* **1967**, *39*, 315-320.